Archives of Materials Science and Engineering

Volume 124
Issue 1
November 2023
Pages 25-41

International Scientific Journal
published monthly by the
World Academy of Materials
and Manufacturing Engineering

DOI: 10.5604/01.3001.0054.3229

Utilising cold sintering process for sintering hydroxyapatite-polyetheretherketone nanocomposite

H.O. Abbas [a,*], H.A. Smeig [a], Z.J.A. Ameer [b]

[a] Department of Materials Engineering, University of Technology, Baghdad, Iraq
[b] Department of Prosthetics and Orthotics Engineering, College of Engineering, Kerbala University, Iraq
* Corresponding e-mail address: Hawraaoday1992@gmail.com
ORCID identifier: https://orcid.org/0000-0002-9052-4451 (H.O.A.)

ABSTRACT

Purpose: A novel technique of very low-temperature sintering named the cold sintering process is used to produce Highly dense hydroxyapatite-polyetheretherketone (HA-PEEK) nanocomposites. The polymers and ceramics are sintered at different temperatures; therefore, it is difficult to create ceramic matrix composites using traditional methods because the high temperatures might damage the polymers. It is hard to concurrently treat polymeric materials at high temperatures because HA often sinters at temperatures exceeding 1000°C. So, the study aimed to use a novel low-temperature sintering named Cold Sintering Process (CSP) with a Ts/Tm ratio greater than 0.2 to alleviate this issue. This method could offer a production path with quick densification and less energy costs to increase throughput.

Design/methodology/approach: In the current work, two different routes are used: The direct mixing and dissolution methods were used for powder preparation to fabricate a unique ceramic matrix composite. The study aimed to determine whether the preparation method could produce two continuous phases for better densification. The sintering temperature, pressure, holding time, and PEEK content were selected as the production parameters. The samples are characterised using a scanning electron microscope (SEM), X-ray energy dispersive spectrometry (EDS), an X-ray diffractogram (XRD), and a transition electron microscope (TEM). Also, physical and mechanical property measurements were detected, including density, water contact angle, hardness, and diametral tensile strength (DTS).

Findings: It can be observed that a high densification compact (relative density 99.3%) can be observed by using the dissolution method HA-PEEK composites, which can be produced via the cold sintering process. The dissolution method can produce two continuous phases compared with the direct mixing method. All samples exhibit excellent hydrophilicity, which makes them good candidates for biomedical applications.

Research limitations/implications: The biggest implication of the cold sintering method is the difficulty of making large-sized and complex-shaped samples.

Practical implications: The dissolution method can produce two continuous phases compared with the direct mixing method. All samples exhibit excellent hydrophilicity, which makes them good candidates for biomedical applications.

Originality/value: A novel technique was used for the first time to solve the problem of producing ceramic matrix composites with polymer as the dispersion phase.

Keywords: Cold sintering process, PEEK, Hydroxyapatite, Two continuous phases, Ceramic composites

Reference to this paper should be given in the following way:

H.O. Abbas, H.A. Smeig, Z.J.A. Ameer, Utilising cold sintering process for sintering hydroxyapatite-polyetheretherketone nanocomposite, Archives of Materials Science and Engineering 124/1 (2023) 25-41. DOI: https://doi.org/10.5604/01.3001.0054.3229

BIOMEDICAL AND DENTAL MATERIALS AND ENGINEERING

1. Introduction

The most popular high-temperature thermoplastic polymer utilised in the biomedical industry, particularly for an interbody fusion cage, is polyetheretherketone (PEEK) [1]. PEEK has good stability in the sterilising process, chemical resistance, and high-temperature resistance because to the aromatic backbone molecular chains that make up its chemical structure. PEEK is furthermore radiolucent, wear-resistant, and biocompatible [2]. PEEK reduces the normal stress-shielding effect that metal implants cause because of its elastic modulus, which is like human cortical bone. Because PEEK is physiologically inert and hinders complete integration with the neighbouring bone, so; it does not immediately connect to the bone after implantation [3]. Synthetic hydroxyapatite (HA), which has the molecular formula $Ca_{10}(PO_4)_6(OH)_2$, is the pure synthetic alternative for human bone mineral [4,5]. HA is a great option for biomedical applications as a bone substitute because of its osteoconductive properties and osteointegration [6-8]. Developing polymeric composites for a load-bearing application (hard tissue) has recently attracted much scientific interest [1]. HA-PEEK is one of the best options for them due to the combination of high mechanical properties for PEEK and strong bioactivity for hydroxyapatite [9]. To produce HA-PEEK composites containing ceramic materials distributed in the polymeric matrix, many traditional methods have been employed, including compounding and injection moulding [10-13], compression moulding [14,15], pressureless sintering [16-18], and selective laser sintering (SLS) [19-22]. Because polymers and ceramics are sintered at different temperatures, creating ceramic matrix composites using any of the methods outlined is difficult because the high temperatures might damage the polymers. It is hard to concurrently treat polymeric materials at temperatures because HA often sinters at temperatures exceeding 1000°C. A novel low-temperature (~300°C) sintering method named Cold Sintering Process (CSP) with a Ts/Tm ratio greater than 0.2 can solve this problem. Such a method could offer a production path with quick densification and less energy costs to increase throughput [23-25].

In the Cold Sintering Process (CSP), a transient phase, frequently liquid or a liquid mixer, aids mass transport. First, the powder was mixed with the liquid phase, and the wetted powder was put in the die. the powder in the die is subjected to uniaxial pressure, which promotes particle rearrangement. A dissolution-precipitation process began after the temperature was raised to between 100 and 300°C in the presence of pressure and a temporary liquid phase. creating the possibility for grain growth and densification [26]. Due to decreasing ceramic sintering temperatures, polymers, nanoparticles, and metals may now be included in ceramic matrix composites. The biggest benefit of CSP technique is that it makes possible to build innovative composite materials with special properties, including ZnO-PTFE [27], $Na_{0.5}Bi_{0.5}MoO_4$-Li_2MoO_4 [28], ZnO-PDMS [29], ZnO-$BaTiO_3$ [30], Al_2O_3-NaCl [31], and ZnO-PEEK [23].

Different methods are used to prepare HA, including chemical precipitation, microemulsion techniques, electrodeposition, hydrolysis, chemical vapour deposition, hydrothermal-electrochemical, solid-state, molten salt, neutralisation, and flame synthesis. In the given work, Ha was prepared by chemical precipitation method. HA-PEEK were combined to create composite biomaterials by adding PEEK to HA using two methods (direct mixing and dissolving process). An extensive examination of the relative densities, microstructures, mechanical and physical characteristics was conducted. The results indicate that excellent mechanical and physical properties with the lowest energy and cost can be obtained by the cold sintering technique.

2. Material and experiments

2.1. Materials

Calcium nitrate tetrahydrate [$Ca(NO_3)_2 \cdot 4H_2O$, Fluka, NLT 99%], diammonium hydrogen phosphate [$(NH_4)2HPO_4$, Fluka, NLT 99%], ammonium hydroxide solution [NH_4OH, Fluka, Min. 28%], hydrochloric acid [HCl, Fluka, Min. 37%] were used as such without further purification. Acetic acid, toluene, and tetrahydrofuran (99%) were obtained from Sinopharm Chemical Reagent Co., Ltd.

PEEK, with an average particle size of 8 µm (~99%), ethanol [C_2H_6O, Qualigenes, NLT 99.5%] was purchased from Jilin Jointure Polymer co., Ltd.

2.2. Synthesis of nano-HA

Nano-HA powders used in the given work were mainly synthesised via the chemical precipitation method, as shown in Fig. 1. By dissolving the desired amount of diammonium hydrogen phosphate (APH, 0.100M) and calcium nitrate (CN, 0.167 M) in double distilled water at 25°C using magnetically stirring for 45 min. A digital pH meter (Systronics 335, India) was used to measure the pH of the prepared solutions. Concentrated NH_4OH was used to adjust the pH of these solutions to 10.5-11 in all experiments. With continuous stirring, 100 ml of the CN solution was slowly added dropwise to 100 ml of the APH solution. The white precipitate was subjected to aqueous washes followed by methanol washes after ageing for a specific duration at 25°C. The resulting gel was oven-dried in the air at 120°C.

2.3. Synthesis of HA-PEEK powders

In the study, HA and PEEK powders were mixed using two methods. The first technique (direct mixing method) for preparing HA-PEEK powders is illustrated in Figure 2b. HA and PEEK powders were blended uniformly in ethanol by magnetic stirring; then, the solution ball was milled Using a planetary ball mill with a rotational speed of 450 revs/min. The combined solution was then in the oven and dried for 6 hours at 90°C. Finally, the dried powder was passed by a mesh (800) screen.

The second technique of mixing involved dissolving the PEEK powders in the solution before distributing the HA powders throughout it. First, 110 mL of toluene and 100 mL of tetrahydrofuran (THF) were combined and stirred magnetically at 400 revolutions per minute for 40 min. The PEEK powders were then added to the mixture at a ratio of 0.40 g/100 mL and stirred magnetically for one hour at 40°C. The temperature was then raised to 71°C, and the stirring continued for 3 hours. The HA nanoparticles were added to the combined solution and agitated for 1.5 hours at 71°C. The combined solution was then mechanically ground using a planetary ball mill for 4 hours with a rotating speed of 1000 rev/min. The mixed solution was then dried at 90°C for 6 hours. An 800-mesh screen was used for sieving the HA-PEEK powders. Figure 2a. show the steps in detail. Table 1 lists the weight percentages of all the compositions, among which HA, HP1- HP4, and D stand for pure HA, HA-PEEK using the direct mixing method (The first mixing route), and HA-PEEK using the dissolution method (The second mixing route).

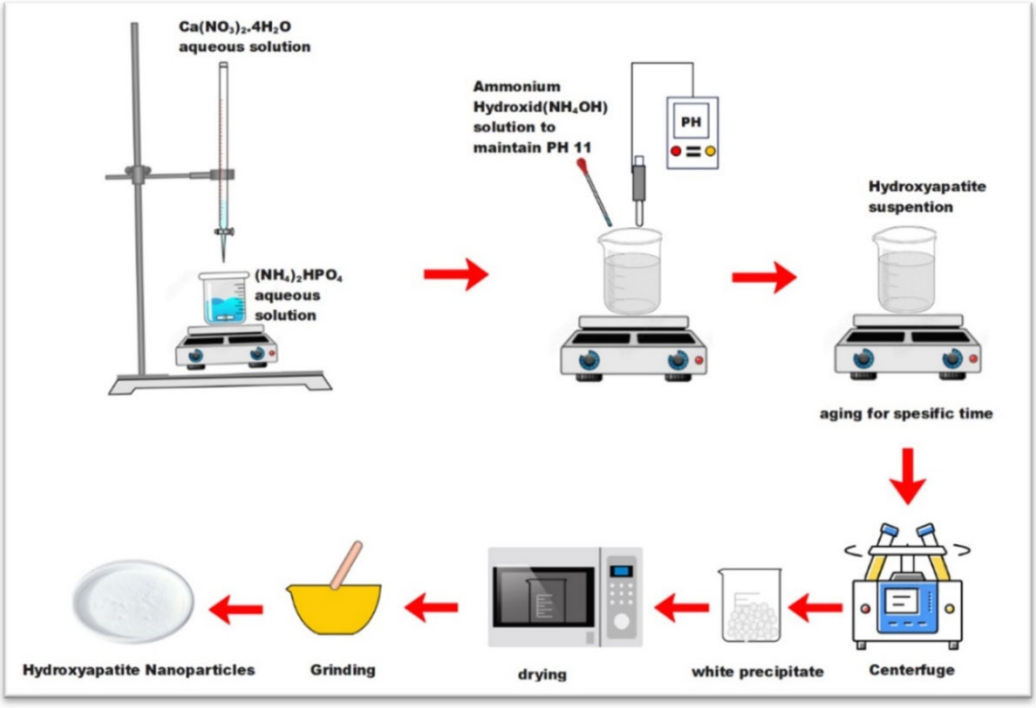

Fig. 1. Schematic illustrating the co-precipitation method for preparing nano-HA

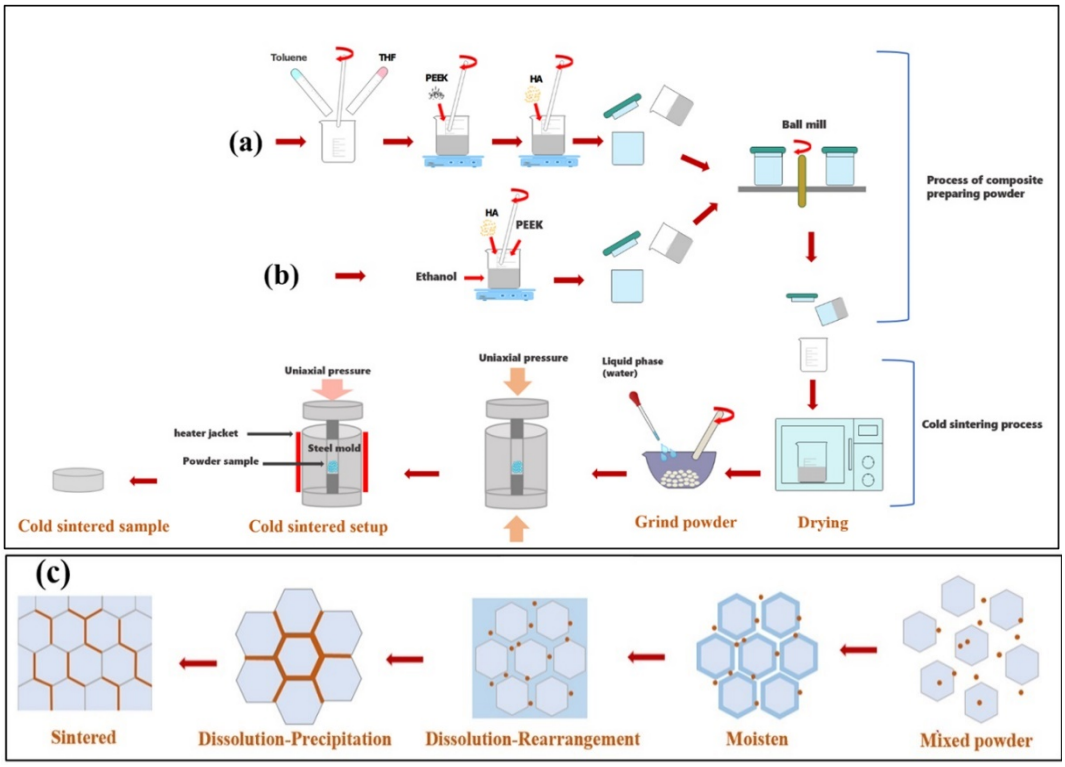

Fig. 2. Schematic illustrating the cold sintering process of composite as well as the mixing routes for nano-HA-PEEK powders: a) dissolution approach (D), b) direct mixing approach, c) mechanism of cold sintering process

Table 1.
Compositions of HA-PEEK powder

Samples	HA, wt.%	PEEK, wt.%
Pure HA	100	0
D	90	10
HP_1	90	10
HP_2	80	20
HP_3	70	30
HP_4	60	40

2.4. Cold sintering process

Figure 2 Shows the schematic illustrating the cold process and mechanism of the composite, where 1g nano-HA-PEEK powders are wetted using 1.5 mol/L aqueous solution (0.12 g) of acetic acid. After being mixed using an agate mortar, the wet powders were placed into a steel die; for composite samples, the die was heated to 300°C at a rate of 5°C/min and pressed under a uniaxial pressure of 500 MPa for 60 minutes before the sample was allowed to cool naturally to 25°C. For the production of pure HA, the powders were wet with (10 wt.%) deionized water, then pressed under 500 MPa pressure and cold sintered for 60 minutes at 250°C.

2.5. Chemical and morphological characterization

Functional groups of the prepared nano-HA powders and nano-HA-PEEK composites were identified by Fourier transform infrared spectrometry (FT-IR, Magna-IR 750, Nicolet, USA). The spectra were recorded from 4000 cm^{-1} to 400 cm^{-1}. X-ray diffraction (XRD, Shimadzu, Japan) using a Cu target is used to examine the crystalline phases of nano-HA powders and nano-HA-PEEK composites. The diffraction angles (2Θ) were set between 10 and 60. Phases were identified by comparing the sample diffraction pattern with reference cards from the ICDD-JCPDS database.

TEM test was used to show the grain size and shape. Before the TEM test, the sample is dissociated using a dissociator and then sonicated by a probe sonicator. After that, take a small amount of your sample, drop 1-2 drops on the TEM grid and leave it to dry at room temperature. To get the best result and to avoid agglomeration of particles.

A field emission scanning electron microscope (FE-SEM, JSM-6701F, JEOL, Tokyo, Japan) characterises the surface morphology of pure nano-HA and the optimum nano-HA-PEEK composite surfaces. Before FE-SEM observation, all samples were coated with gold for 1 minute.

Energy dispersive X-ray spectroscopy (EDS) was also recorded using the same equipment to confirm the element in the prepared sample and help calculate the Ca/p ratio after immersion in SBF for 14 days.

2.6. Mechanical properties

The diametral tensile strength (DTS) of the sintered HA samples was found by compressing each sample (12mm diameter and 5mm thickness) using a universal test instrument (Instron 5500R, USA), which was placed on its side between the two plates of Instron 5500R machine, at a crosshead speed of 0.5 mm/min until failure. The DTS (MPa) was calculated from the equation:

$$DTS = \frac{2F_{max}}{\pi.t.d} \quad (1)$$

where F_{max} is the failure load, d is the diameter, and t is the thickness of the sample.

Vickers microhardness (HV) was also tested using Shimadzu Microhardness Tester (HMV-2L). A force (P) with a 1.961 N load and 15 s dwell time to obtain an indentation with crack propagation. Six locations were selected and measured for each sample, taking an average value.

A contact angle measuring device (SL200B, Kono, USA) is utilised to measure the contact angles of pure nano-HA and the optimum nano-HA-PEEK composite surfaces using the sessile drop method with a 2 mL D.I. water droplet measured at room temperature. In order to provide an average and standard deviation, six samples in each stage were used.

Archimedes' principle, as described in the ASTM B 311-08 standard, was used to calculate All sample densities using the following formula:

$$RD = \frac{\rho}{\rho_c} \times 100 \quad (2)$$

where:
RD = Relative density (%);
ρ = Experimentally measured density (gr/cm^3);
ρ_c = Theoretical density calculated based on powder mixture ratios (gr/cm^3).

$$\rho_c = \frac{1}{\left(\frac{M}{\rho_m}\right)+\left(\frac{R}{\rho_r}\right)} \quad (3)$$

M equals (Wm/C), the weight per cent of the matrix, and R equals (Wr/WC), the weight per cent of reinforcement. Equation (2) can be used to estimate the true density of the composite using the weight per cent of the matrix and the reinforcement as well as their theoretical densities. In the case of HA-PEEK nanocomposites, the theoretical density of HA is 3.219 g/cm^3, and for PEEK, it is equal to 1.28 g/cm^3.

3. Results and discussions

3.1. Characterisation of nano-HA crystals

The apatite phase was proven to exist in nano-HA crystals by Fourier transform infrared spectroscopy, as illustrated in Figure 3b. The stretching and vibrational modes of OH^- ions cause the bands at 3572 cm^{-1} and 631 cm^{-1}, respectively. The bands at 1090 cm^{-1} and 1040 cm^{-1} are caused by v3 PO4, the band at 962 cm^{-1} is caused by v1 PO_4, and v4 PO_4 causes the bands at 601 cm^{-1} and 574 cm^{-1}. The 2200 cm^{-1} to 1950 cm^{-1} range has a collection of weak intensity bands that result from overtones and combinations

a)

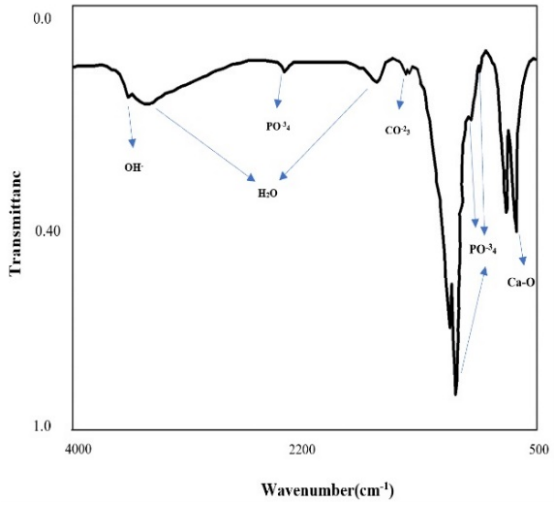

b)

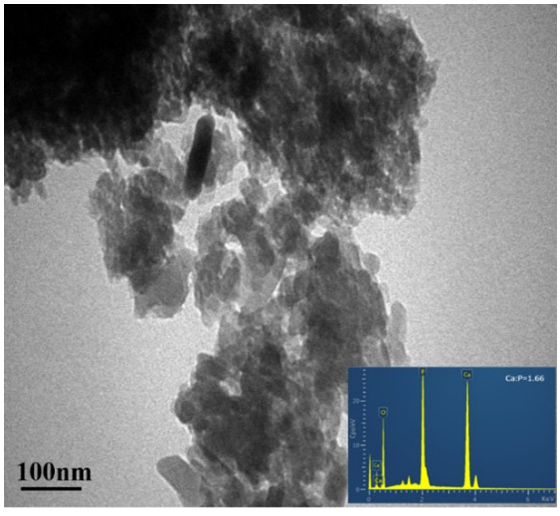

Fig. 3. Characterisation of nano-hydroxyapatite prepared by co-precipitation method: a) FTIR, b) TEM

of the v1 and v3 PO_4 modes. The sharpness of the bands shows the well-crystallinity of the produced nanoparticles. The discovery and the information from TEM suggest that the produced particles are nanomaterials. The adsorbed water is related to the characteristic wide peak at 3435 cm^{-1} and 1640 cm^{-1}. The presence of the OH group in apatite might cause the weak band at 3570 cm^{-1} [32]. TEM observed morphologies of the obtained HA nanocrystals. Figure 3a showed an aggregate of nanoparticles with different c/a ratios, all having a size of less than 100 nm. The average crystallite sizes were 17 nm, calculated using the Image J program. Pure HA nanoparticles strongly tended to form agglomerates due to their high surface area and surface energy.

3.2. Composition and morphology of the cold sintered nano-HA

XRD patterns of the sintered HA nanopowders revealed the production of apatite as a single phase with no additional impurity phases, as shown in Figure 4a. Each pattern matches ICDD Card 01-089-6439. Using the Scherrer formula and the full width at half maximum (FWHM) peak corresponding to the (002) plane, which is independent and does not interfere with other peaks, the average crystallite size was determined to be 75.9 nm.

The surface morphology of the cold-sintered HA was characterised using SEM to evaluate the sample microstructure.

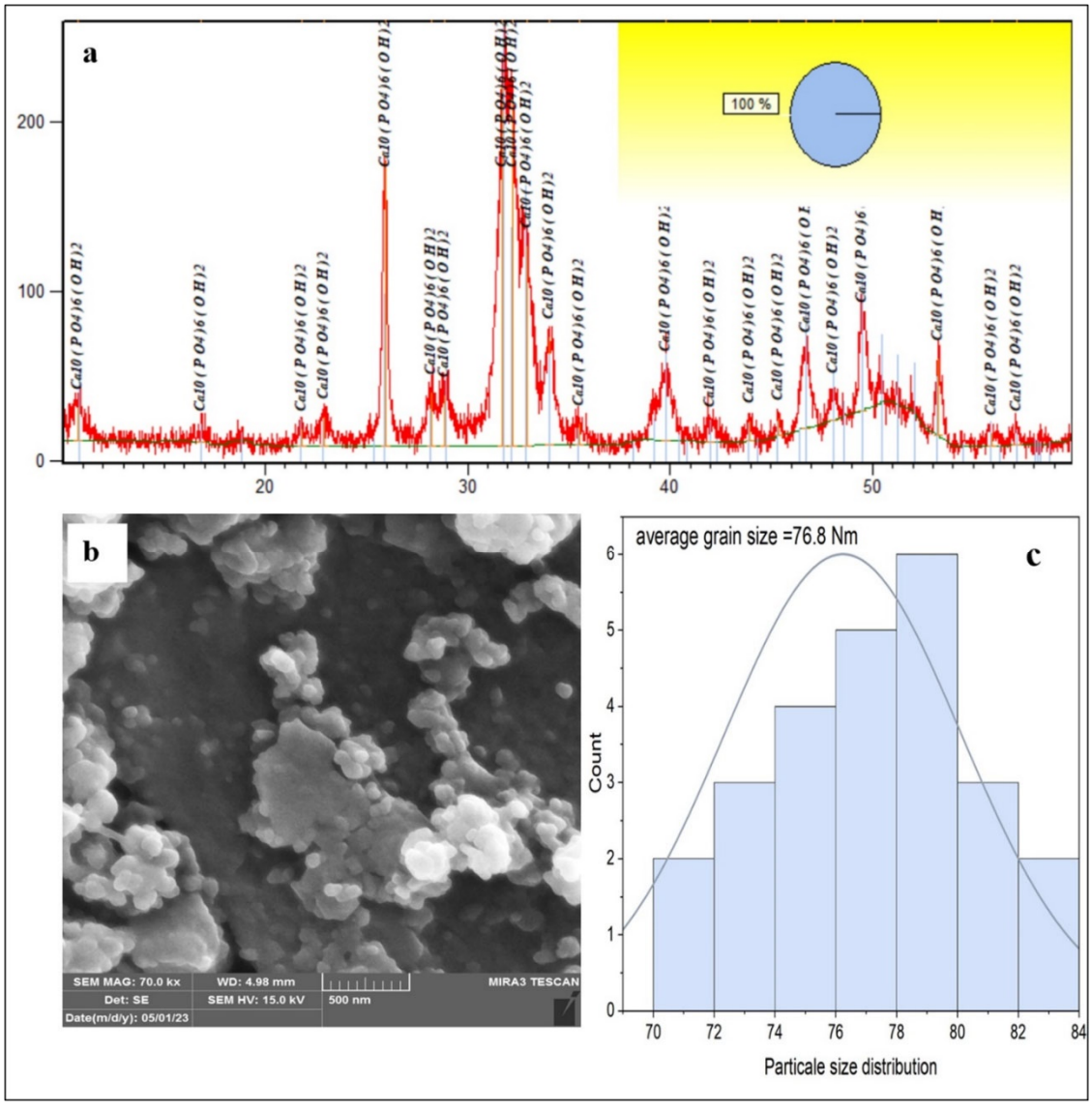

Fig. 4. Characterisation of the cold sintered nano-hydroxyapatite: a) XRD, b) SEM, and c) particle size distribution

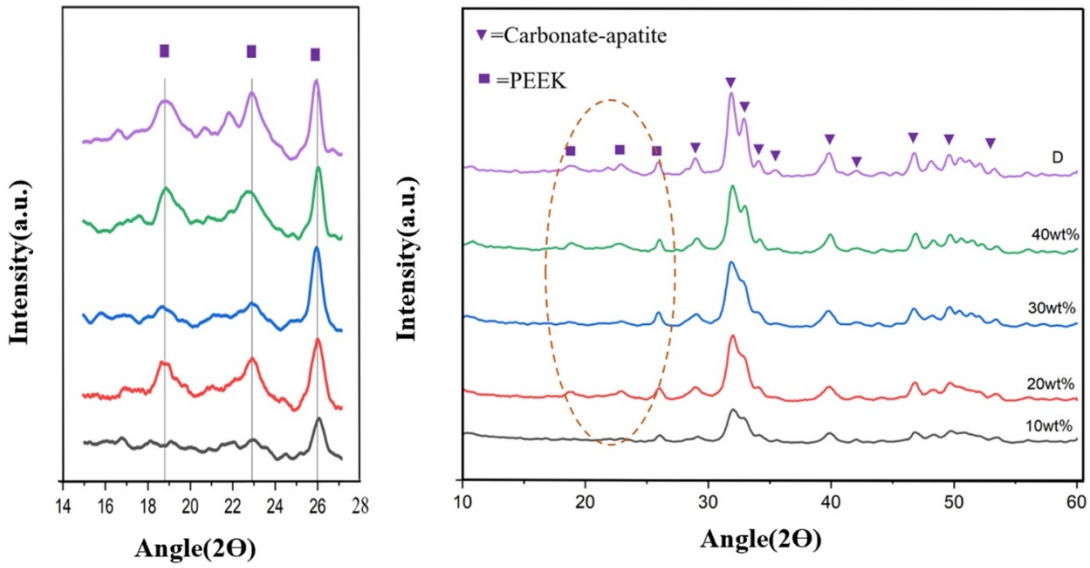

Fig. 5. XRD patterns of the cold-sintered nano-HA-PEEK composite (10, 20, 30, 40 wt.% PEEK content and D sample)

Figure 4b shows that the sample consists of agglomerated spheroidal particles smaller than 100 nm. It can be distinguished that the surfaces of the CSP-sintered sample consist of Spherical structures with smaller particles. The average particle size of the cold-sintered sample estimated by the Image J program was 75. at the same time, 17 nm was the initial particle size of HA powder, which approved the grain growth and densification of the CSP-sintered sample. The SEM results agree with the HA relative density (99%), indicating a highly dense sample can be obtained by the cold sintering process.

3.3. Composition and morphology of nano-HA--PEEK composite

Figure 5 reveals the XRD patterns of the cold-sintered nano-HA-PEEK composite samples. The sharp peaks belong to carbonated apatite, whereas the weak peaks are typical of PEEK polymer. The nano-HA particles partially encapsulating the PEEK surface reduced the intensity of the PEEK main peaks in the nano-HA-PEEK composite. The formation of B-type carbon-substituted apatite is caused by the ion exchange in the crystal structure of HA during the composite preparation process. It is similar to the apatite located in the bone [33].

SEM images of cold-sintered HA-PEEK composites are shown in Figures 6, 7, 8, 9, and 10. Two distinct phases are evident in all samples, revealing dense microstructures in conformity with the XRD results (Fig. 5). Large PEEK particles are not noticeable when using the dissolution method (D) because PEEK particles with 10 Mm are uniformly dissolved in the THF and toluene solutions, allowing for the uniform distribution of small PEEK particles along the HA grains. In the instance of the direct mixing approach, it was also found out that large particles (PEEK) were present. In addition, small HA particles may cover the PEEK grains in some areas. PEEK particles become more and more unevenly distributed as PEEK content increases. The relative densities tend to decrease as the PEEK content increases because some pores may be detected in the microstructure as PEEK increases, which is in good accord with the density data. It is because the PEEK particles are between the HA grains, which may hinder the mass transport grain growth of the HA particles.

In summary, the dissolved method produced a uniform distribution of small PEEK particles along the HA grains compared with the direct mixing method. To determine whether the samples have a continuous phase or not. The samples were etched in HCl because PEEK had a higher chemical resistance to HCl than HA.

Figure 11c. Unlike the dissolution method (D), the sample maintains its crystal structure. It does not cause any collapse when immersed in HCl for three days, as shown in Figure 11a. It is homogeneously distributed along the HA grains, forming a continuous phase. It has been observed that the direct mixing method did not form a continuous phase of PEEK due to the irregular distribution of PEEK particles between HA grains. Figure 11b shows the destroyed sample after a few hours of immersion in HCl. After one day of immersion in concentrated acid, the sample was destroyed.

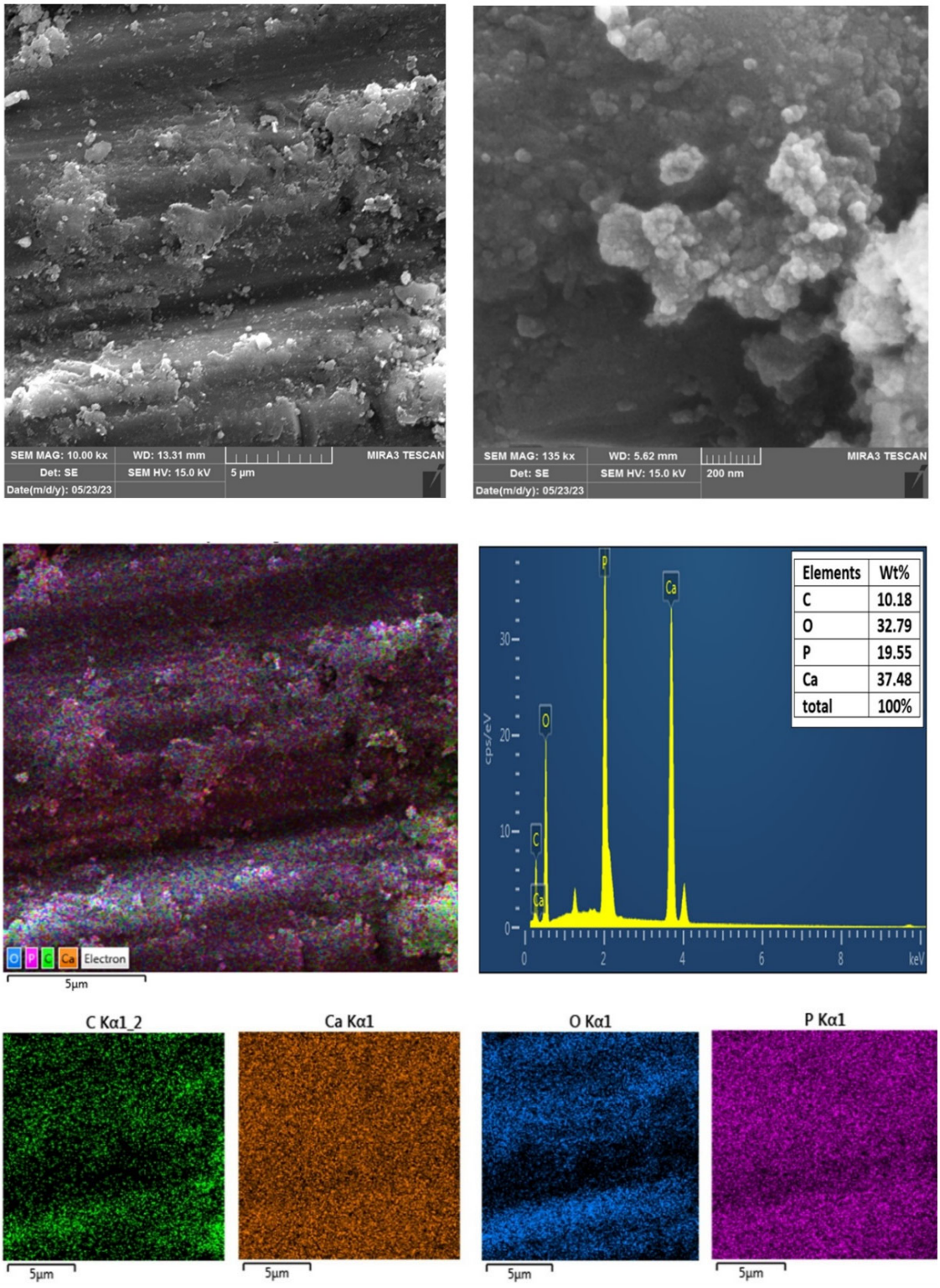

Fig. 6. SEM image at different magnification of 10 wt.% HA-PEEK composite sample (a, b), (c, d and e) EDS mapping and EDS spectra of sample

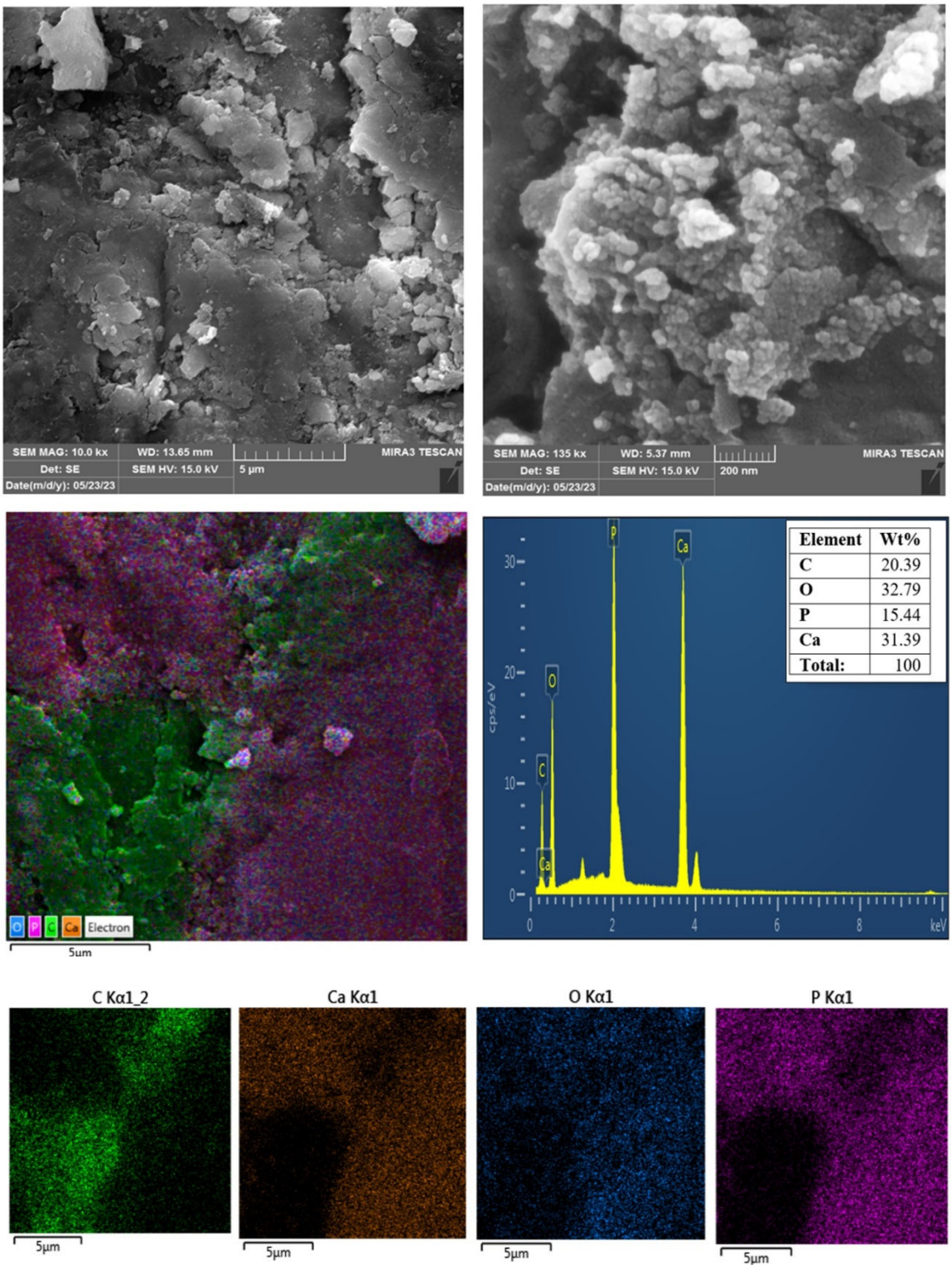

Fig. 7. SEM image at different magnification of 20wt% HA-PEEK composite sample (a, b), (c, d and e) EDS mapping and EDS spectra of sample

The agreement is with the energy dispersive X-ray spectrum (EDS) analysis, where the green and purple contrast regions belong to the PEEK and HA phases. Figures 6, 7, 8, and 9 show the PEEK (green) distributed along the

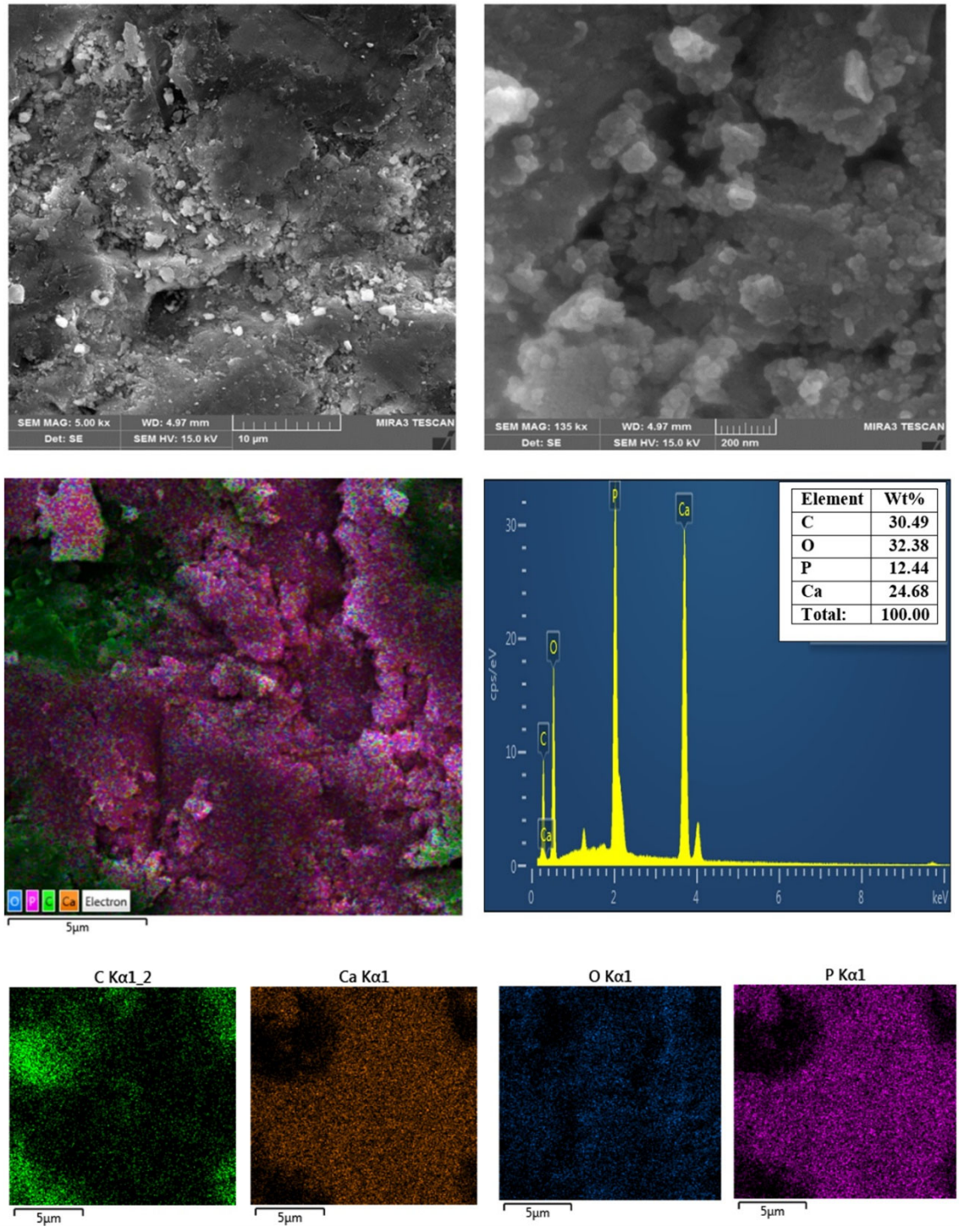

Fig. 8. SEM image at different magnification of 30wt% HA-PEEK composite sample (a, b), (c, d and e) EDS mapping and EDS spectra of sample

HA grains (purple) without a continuous phase. In contrast to Figure 10, the PEEK grains (green) are homogeneously distributed along the HA grain boundary, forming the continuous phase.

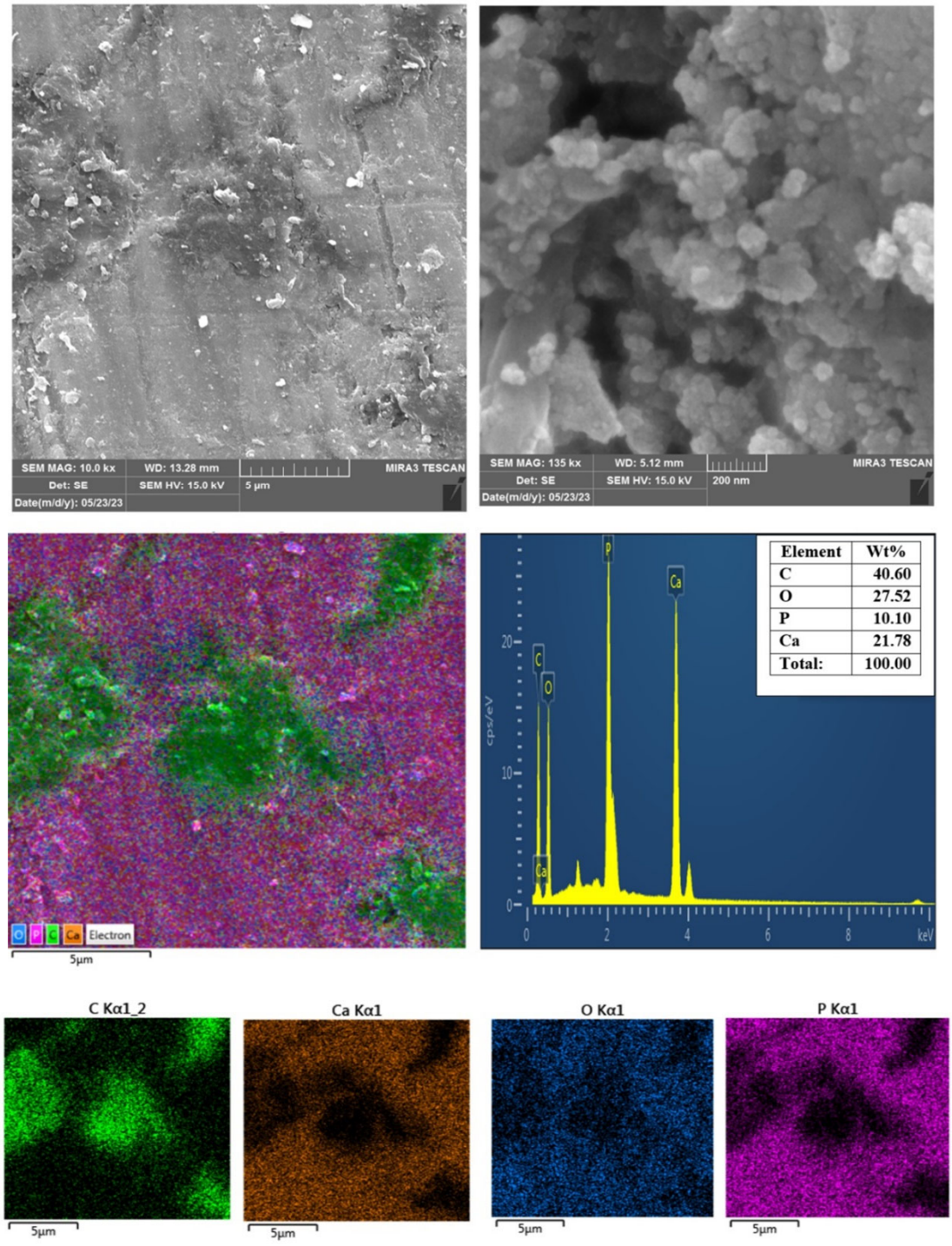

Fig. 9. SEM image at different magnification of 40wt% HA-PEEK composite sample (a, b), (c, d and e) EDS mapping and EDS spectra of sample

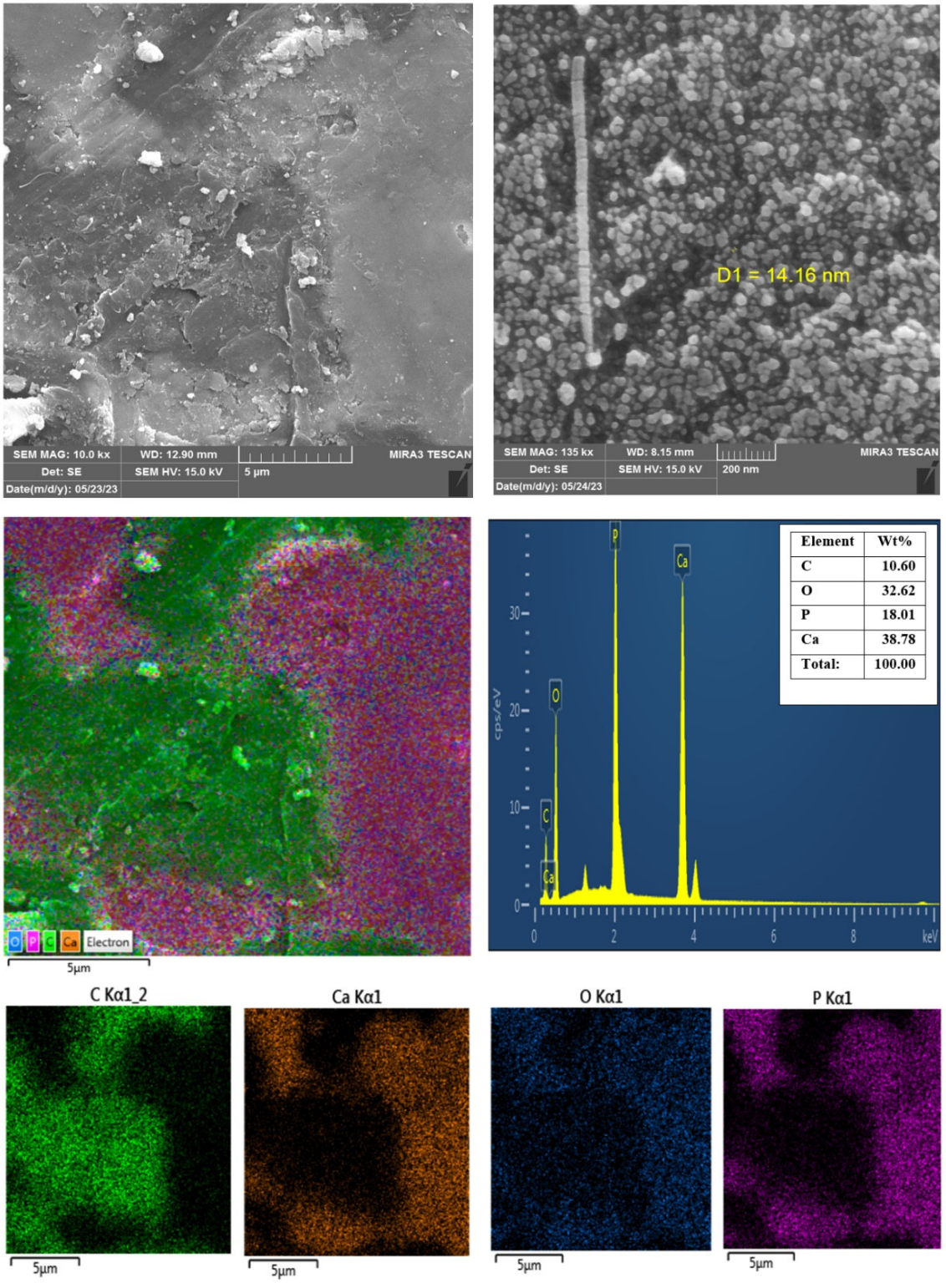

Fig.10. SEM image at different magnification of (D) sample (a, b). (c, d and e) EDS mapping and EDS spectra of HA-PEEK composite sample

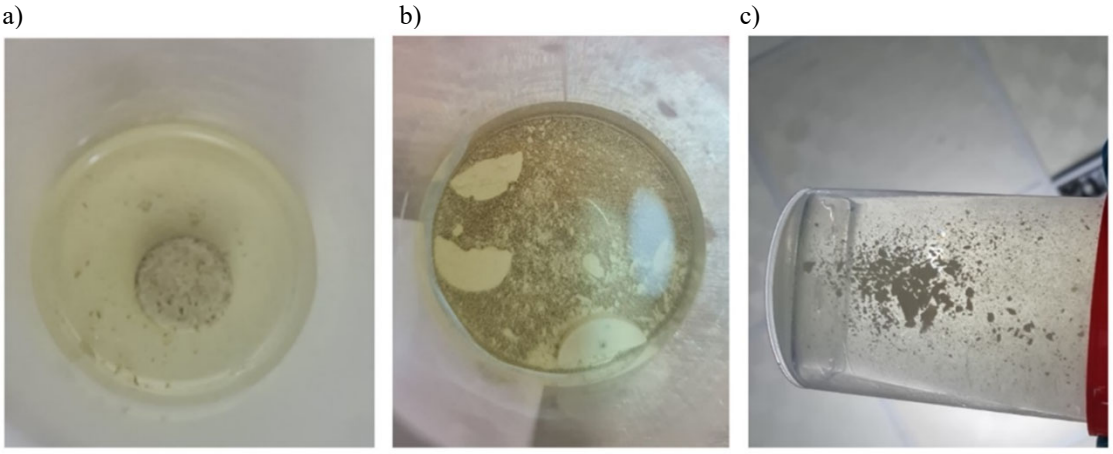

Fig. 11. HA-PEEK sample immersed in HCl: a) D sample after 3 days, b) 10 wt.% after few hours in HCl, c) 10 wt.% after one day

3.4. Density results

Based on several experiments, the Taguchi method was used to determine the optimal conditions (sintering temperature of 300°C, sintering pressure of 250 bar, holding time of 60 min, and heating rate of 5°C/min). Under such conditions, the samples were able to reach high relative densities. The relative densities of all samples range between 79% and 99%, indicating that the cold sintering process can obtain the highly dense nano-HA-PEEK composites. As shown in Figure 12, the densities of the ceramic–polymer composites decrease with increasing amounts of polymer. Because the density of PEEK polymer is lighter (1.281 g/cm^3) than the density of HA ceramic (3.21 g/cm^3). It can be observed the D sample has a high relative compared with the the same PEEK content sample produced by the direct mixing method. The density results confirm the SEM results, where the PEEK is well distributed in the HA matrix, leading to better densification. Time and temperature are significant factors in the dissolution of soluble substances. As shown in Figure 2c, time and temperature are required to move the particles into the pores.

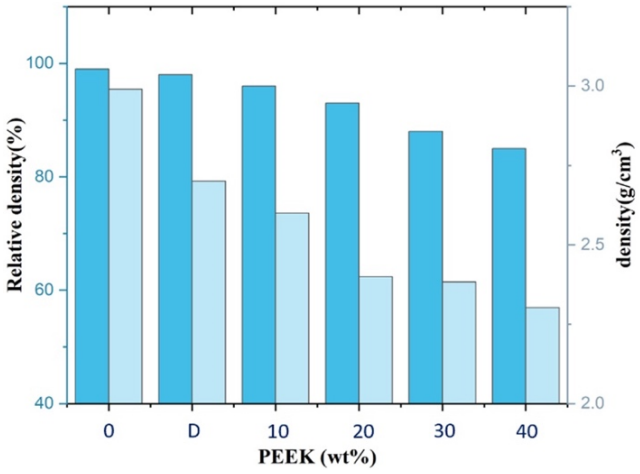

Fig. 12. The densities and relative densities of the HA-PEEK composites with the amount of PEEK ranging from 0 to 40 wt.%

Particle rearrangement occurs via the liquid medium and pressure during the initial cold sintering process. The second stage(dissolution-precipitation process) involves dissolving particles under temperature and pressure, which leads to the formation of a supersaturated phase leading to the nucleation and densification (grain growth) of the powder. Therefore, the optimum temperature and time are essential for the successful cold-sintering densification of composites [23].

3.5. Mechanical propertes results

Figure 13. shows the results of diametral tensile property and Hardness varus PEEK content. It can be observed as amount of PEEK (from 0 to 40%) increased the diametral tensile strength increase.

The sample prepared by dissolved method (D) have higher diametral tensile strength compared with sample prepared by direct mixing method with same percentage (10 wt.% PEEK content). It is due to the homogeneous distribution of HA and PEEK in the sample which confirm the SEM results. The two continuous phases are favourable in composite material in order to obtain better mechanical properties compared with others. As PEEK content increases, the tensile strength of composites increases

because the tensile strength of polymers is higher than that of ceramic. Also, advantage of PEEK is that it is ductile and not as brittle as ceramics [34]. The elastic modulus recorded under these conditions was 5 GPa, which is in the cortical bone elastic modulus range [17].

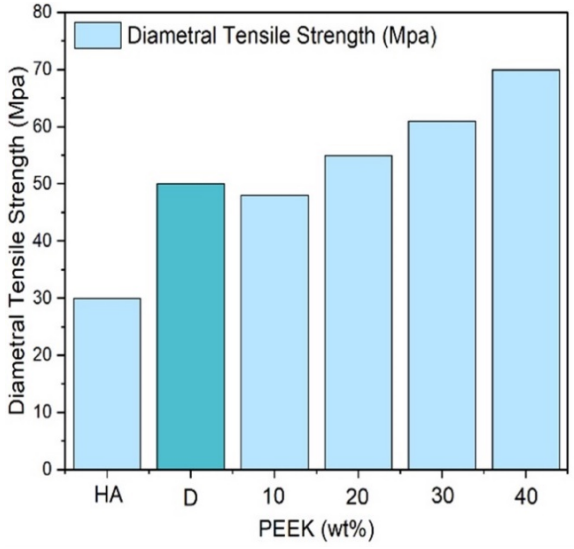

Fig. 13. diametral tensile strength and the hardness of the HA-PEEK composites with the amount of PEEK ranging from 0 to 40 wt.%

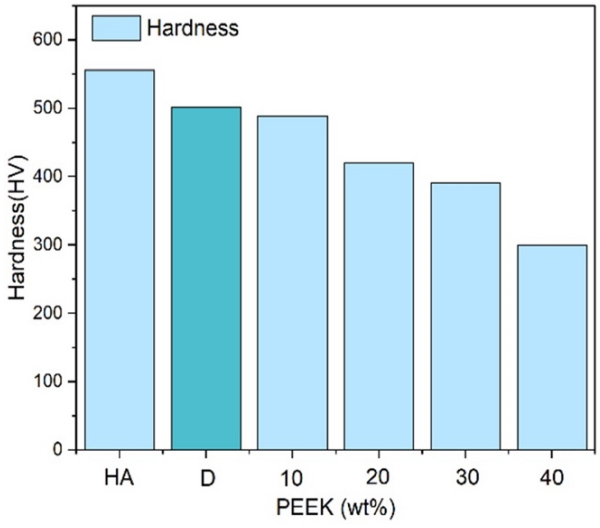

Fig. 14. The hardness of the HA-PEEK composites with the amount of PEEK ranging from 0 to 40 wt.%

Figure 14 shows the hardness of samples varus PEEK content. The hardness decreases gradually as PEEK content increases. Due to the hardness of PEEK being lower than HA hardness, all sample hardness results in the range of cortical bone hardness.

3.6. Contact angle result

The water contact angle is a convenient way to assess the wettability and biocompatibility of composite surfaces [35]. Figure 15. shows the contact angles of pure HA and the composite, respectively. The pure HA possessed the lowest contact angle of approximately 28°, corresponding to the highest surface hydrophilicity. Measured contact angles at D and 10%, 20%, 30%, 40% PEEK samples were 34°, 31°, 40°,47°, and 53° respectively. It can be noticed that all samples exhibit good hydrophilic properties because of their hydrophilicity, which is attributed to the existence of -OH groups on their surface. The nano-HA-PEEK composite does not affect the hydrophobicity of PEEK, and it remains hydrophilic due to the HA particles partially covering the PEEK surface. In order to attain great surface coverage (hydrophilic), a low contact angle is often preferable.

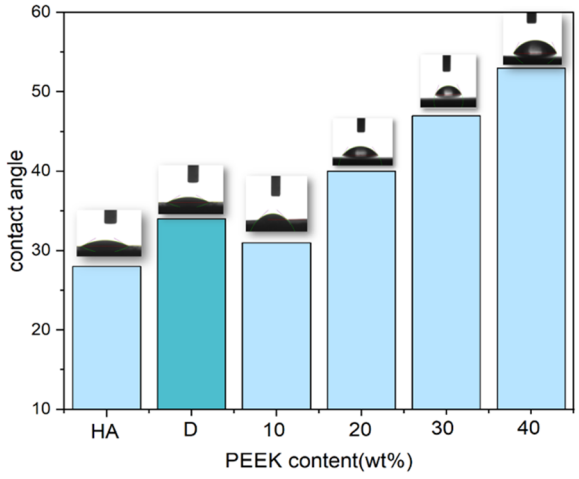

Fig. 15. The contact angle of the HA-PEEK composites with the amount of PEEK ranging from 0 to 40 wt.%

It has been demonstrated that the maximum degrees of cell attachment, protein adsorption, platelet adhesion/ activation, and blood coagulation are stimulated by hydrophilic surfaces.

4. Conclusions

In the study, a novel technique named the Cold sintering process shows the ability to produce composite material with high-volume fractions of ceramic. A new type of HA-polymer composites is developed. PEEK, a thermoplastic

polymer, was initially incorporated into HA using the cold sintering method. The direct mixing and dissolution methods are powder preparation methods to fabricate a unique composite. Dense HA-PEEK composites may be produced using CSP with a dilute acetic acid solution (1.5 mol/L) at a low temperature of 300°C, pressure of 500 MPa and 60 min holding time. Under such optimum conditions, the composite exhibits the maximum relative density of ~99% with the addition of 10 wt.% PEEK. In the case of the dissolution procedure, PEEK can be uniformly dissolved by a solution of tetrahydrofuran and toluene, forming a tiny particle of PEEK in the samples. PEEK particles can be homogeneously distributed along the HA grain boundaries after the cold sintering process. In the case of the direct mixing approach, Many of the PEEK particles are similar in size to the raw powders after the cold sintering process. The dissolution method can produce two continuous phases compared with the direct mixing method. Highly dense samples with good mechanical properties and excellent hydrophilicity make them good candidates for biomedical applications. In conclusion, the study offers two methods to produce functional HA-PEEK composites, which could inspire future research on cold-sintered ceramic-polymer composites.

Acknowledgements

Special thanks and gratitude are extended to the Department of Material Engineering, University of Technology, Iraq.

References

[1] R. Ma, T. Tang, Current strategies to improve the bioactivity of PEEK, International Journal of Molecular Sciences 15/4 (2014) 5426-5445. DOI: https://doi.org/10.3390/ijms15045426

[2] D. Briem, S. Strametz, K. Schröoder, N.M. Meenen, W. Lehmann, W. Linhart, A. Ohl, J.M. Rueger, Response of primary fibroblasts and osteoblasts to plasma treated polyetheretherketone (PEEK) surfaces, Journal of Materials Science: Materials in Medicine 16/7 (2005) 671-677. DOI: https://doi.org/10.1007/s10856-005-2539-z

[3] R. Ma, D. Guo, Evaluating the bioactivity of a hydroxyapatite-incorporated polyetheretherketone biocomposite, Journal of Orthopaedic Surgery and Research 14/1 (2019) 32. DOI: https://doi.org/10.1186/s13018-019-1069-1

[4] W. Akram, R. Zahid, R.M. Usama, S.A. AlQahtani, M. Dahshan, M.A. Basit, M. Yasir, Enhancement of Antibacterial Properties, Surface Morphology and In Vitro Bioactivity of Hydroxyapatite-Zinc Oxide Nanocomposite Coating by Electrophoretic Deposition Technique, Bioengineering 10/6 (2023) 693. DOI: https://doi.org/10.3390/bioengineering10060693

[5] S. Kowalski, R. Belka, W. Żórawski, M. Sztorc, A. Góral, M. Makrenek, Microstructural study of plasma sprayed hydroxyapatite coatings, Journal of Achievements in Materials and Manufacturing Engineering 83/2 (2017) 79-84. DOI: https://doi.org/10.5604/01.3001.0010.7035

[6] T. Kokubo, H.M. Kim, M. Kawashita, Novel bioactive materials with different mechanical properties, Biomaterials 24/13 (2003) 2161-2175. DOI: https://doi.org/10.1016/S0142-9612(03)00044-9

[7] S. Bashar, H. A. Al-Kaisy, and M. N. Al-Shroofy, Preparation of Bio-Composite Coatings on Titanium Substrate by Electrostatic Spray Deposition, Key Engineering Materials 937 (2022) 129-138. DOI: https://doi.org/10.4028/p-224uc8

[8] M.N. Obaid, O.H. Sabr, A.A. Hussein, Characteristic of polypropylene nanocomposite material reinforcement with hydroxyapatite for bone replacement, Journal of Achievements in Materials and Manufacturing Engineering 104/1 (2021) 21-30. DOI: https://doi.org/10.5604/01.3001.0014.8483

[9] R. Ma, L. Weng, X. Bao, Z. Ni, S. Song, W. Cai, Characterization of in situ synthesized hydroxyapatite/polyetheretherketone composite materials, Materials Letters 71 (2012) 117-119. DOI: https://doi.org/10.1016/j.matlet.2011.12.007

[10] M.S. Abu Bakar, M.H.W. Cheng, S.M. Tang, S.C. Yu, K. Liao, C.T. Tan, K.A. Khor, P. Cheang, Tensile properties, tension-tension fatigue and biological response of polyetheretherketone-hydroxyapatite composites for load-bearing orthopedic implants, Biomaterials 24/13 (2003) 2245-2250. DOI: https://doi.org/10.1016/S0142-9612(03)00028-0

[11] S.M. Tang, P. Cheang, M.S. AbBakar, K.A. Khor, K. Liao, Tension-tension fatigue behavior of hydroxyapatite reinforced polyetheretherketone composites, International Journal of Fatigue 26/1 (2004) 49-57. DOI: https://doi.org/10.1016/S0142-1123(03)00080-X

[12] K.L. Wong, C.T. Wong, W.C. Liu, H.B. Pan, M.K. Fong, W.M. Lam, W.L. Cheung, W.M. Tang, K.Y. Chiu, K.D.K. Luk, W.W. Lu, Mechanical properties and in vitro response of strontium-containing hydroxyapatite/polyetheretherketone composites,

Biomaterials 30/23-24 (2009) 3810-3817. DOI: https://doi.org/10.1016/j.biomaterials.2009.04.016
[13] R. Ma, S. Tang, H. Tan, W. Lin, Y. Wang, J. Wei, L. Zhao, T. Tang, Y. Pan, Preparation, characterization, and in vitro osteoblast functions of a nano-hydroxyapatite/polyetheretherketone biocomposite as orthopedic implant material, International Journal of Nanomedicine 9/1 (2014) 3949-3961. DOI: https://doi.org/10.2147/IJN.S67358
[14] G.L. Converse, W. Yue, R.K. Roeder, Processing and tensile properties of hydroxyapatite-whisker-reinforced polyetheretherketone, Biomaterials 28/6 (2007) 927-935. DOI: https://doi.org/10.1016/j.biomaterials.2006.10.031
[15] G.L. Converse, T.L. Conrad, R.K. Roeder, Mechanical properties of hydroxyapatite whisker reinforced polyetherketoneketone composite scaffolds, Journal of the Mechanical Behavior of Biomedical Materials 2/6 (2009) 627-635. DOI: https://doi.org/10.1016/j.jmbbm.2009.07.002
[16] G.L. Converse, T.L. Conrad, C.H. Merrill, R.K. Roeder, Hydroxyapatite whisker-reinforced polyetherketoneketone bone ingrowth scaffolds, Acta Biomaterialia 6/3 (2010) 856-863. DOI: https://doi.org/10.1016/j.actbio.2009.08.004
[17] S. Yu, K.P. Hariram, R. Kumar, P. Cheang, K.K. Aik, In vitro apatite formation and its growth kinetics on hydroxyapatite/ polyetheretherketone biocomposites, Biomaterials 26/15 (2005) 2343-2352. DOI: https://doi.org/10.1016/j.biomaterials.2004.07.028
[18] C. Hengky, B. Kelsen, Saraswati, P. Cheang, Mechanical and biological characterization of pressureless sintered hydroxapatite-polyetheretherketone biocomposite, in: C.T. Lim, J.C.H. Goh (eds), 13th International Conference on Biomedical Engineering, IFMBE Proceedings, vol. 23, Springer, Berlin, Heidelberg, 2009, 261-264. DOI: https://doi.org/10.1007/978-3-540-92841-6_63
[19] F.E. Jabri, A. Ouballouch, L. Lasri, R. El Alaiji, A comprehensive review of polymer materials and selective laser sintering technology for 3D printing, Journal of Achievements in Materials and Manufacturing Engineering 118/1 (2023) 5-17. DOI: https://doi.org/10.5604/01.3001.0053.7286
[20] K.H. Tan, C.K Chua, K.F Leong, C.M Cheah, P Cheang, M.S Abu Bakar, S.W Cha, Scaffold development using selective laser sintering of polyetheretherketone-hydroxyapatite biocomposite blends, Biomaterials 24/18 (2003) 3115-3123. DOI: https://doi.org/10.1016/S0142-9612(03)00131-5
[21] M. Schmidt, D. Pohle, T. Rechtenwald, Selective laser sintering of PEEK, CIRP Annals 56/1 (2007) 205-208. DOI: https://doi.org/10.1016/j.cirp.2007.05.097
[22] K.H. Tan, C.K. Chua, K.F. Leong, M.W. Naing, C.M. Cheah, Fabrication and characterization of three-dimensional poly(ether-ether-ketone)/-hydroxyapatite biocomposite scaffolds using laser sintering, Proceedings of the Institution of Mechanical Engineers, Part H: Journal of Engineering in Medicine 219/3 (2005) 183-194. DOI: https://doi.org/10.1243/095441105X9345
[23] M. Si, J. Hao, E. Zhao, X. Zhao, J. Guo, H. Wang, C.A. Randall, Preparation of zinc oxide/poly-ether-ether-ketone (PEEK) composites via the cold sintering process, Acta Materialia 215 (2021) 117036. DOI: https://doi.org/10.1016/j.actamat.2021.117036
[24] J.-P. Maria, X. Kang, R.D. Floyd, E.C. Dickey, H. Guo, J. Guo, A. Baker, S. Funihashi, C.A. Randall, Cold sintering: Current status and prospects, Journal of Materials Research 32/17 (2017) 3205-3218. DOI: https://doi.org/10.1557/jmr.2017.262
[25] T. Hérisson de Beauvoir, K. Tsuji, X. Zhao, J. Guo, C. Randall, Cold sintering of ZnO-PTFE: Utilizing polymer phase to promote ceramic anisotropic grain growth, Acta Materialia 186 (2020) 511-516. DOI: https://doi.org/10.1016/j.actamat.2020.01.002
[26] S. Funahashi, J. Guo, H. Guo, K. Wang, A.L. Baker, K. Shiratsuyu, C.A. Randall, Demonstration of the cold sintering process study for the densification and grain growth of ZnO ceramics, Journal of the American Ceramic Society 100/2 (2017) 546-553. DOI: https://doi.org/10.1111/jace.14617
[27] T. Hérisson de Beauvoir, S. Dursun, L. Gao, C. Randall, New Opportunities in Metallization Integration in Cofired Electroceramic Multilayers by the Cold Sintering Process, ACS Applied Electronic Materials 1/7 (2019) 1198-1207. DOI: https://doi.org/10.1021/acsaelm.9b00184
[28] D. Wang, D. Zhou, S. Zhang, Y. Vardaxoglou, W.G. Whittow, D. Cadman, I.M. Reaney, Cold-Sintered Temperature Stable $Na_{0.5}Bi_{0.5}MoO_4$-Li_2MoO_4 Microwave Composite Ceramics, ACS Sustainable Chemistry and Engineering 6/2 (2018) 2438-2444. DOI: https://doi.org/10.1021/acssuschemeng.7b03889
[29] A. Ndayishimiye, Z.A. Grady, K. Tsuji, K. Wang, S.H. Bang, C.A. Randall, Thermosetting polymers in cold sintering: the fabrication of ZnO-polydimethylsiloxane composites, Journal of the American Ceramic Society 103/5 (2020) 3039-3050. DOI: https://doi.org/10.1111/jace.17009

[30] L. Coutinho, R.G. Aredes, E. Antonelli, Cold sintering and electric characterization of ZnO-$BaTiO_3$ composites, Ceramica 67/381 (2021) 105-110. DOI: https://doi.org/10.1590/0366-69132021673813061
[31] J. Induja, M.T. Sebastian, Microwave dielectric properties of cold sintered Al_2O_3-NaCl composite, Materials Letters 211 (2018) 55-57. DOI: https://doi.org/10.1016/j.matlet.2017.09.083
[32] N. Guo, H.Z. Shen, Q. Jin, P. Shen, Hydrated precursor-assisted densification of hydroxyapatite and its composites by cold sintering, Ceramics International 47/10 (2021) 14348-14353. DOI: https://doi.org/10.1016/j.ceramint.2021.01.294
[33] Y. Deng, Y. Sun, X. Chen, P. Zhu, S. Wei, Biomimetic synthesis and biocompatibility evaluation of carbonated apatites template-mediated by heparin, Materials Science and Engineering: C 33/5 (2013) 2905-2913. DOI: https://doi.org/10.1016/j.msec.2013.03.016
[34] E. Papia, S.A.C. Brodde, J.P. Becktor, Deformation of polyetheretherketone, PEEK, with different thicknesses, Journal of the Mechanical Behavior of Biomedical Materials 125 (2022) 104928. DOI: https://doi.org/10.1016/j.jmbbm.2021.104928
[35] Y. Zheng, C. Xiong, S. Zhang, X. Li, L. Zhang, Bone-like apatite coating on functionalized poly(etheretherketone) surface via tailored silanization layers technique, Materials Science and Engineering: C 55 (2015) 512-523. DOI: https://doi.org/10.1016/j.msec.2015.05.070